Anthropogenic strath terrace formation caused by reduced sediment retention

Sarah A. Schanz[a,1,2], David R. Montgomery[a], and Brian D. Collins[a]

[a]Department of Earth and Space Sciences, University of Washington, Seattle, WA 98195

Edited by Thure E. Cerling, University of Utah, Salt Lake City, UT, and approved March 13, 2019 (received for review August 24, 2018)

Across North America, human activities have been shown to cause river incision into unconsolidated alluvium. Human-caused erosion through bedrock, however, has only been observed in local and isolated outcrops. Here, we test whether splash-dam logging, which decreased in-stream alluvial cover by removing much of the alluvium-trapping wood, caused basin-wide bedrock river incision in a forested mountain catchment in Washington State. We date incision of the youngest of four strath terraces, using dendrochronology and radiocarbon, to between 1893 CE and 1937 CE in the Middle Fork Teanaway River and 1900 CE and 1970 CE in the West Fork Teanaway River, coincident with timber harvesting and splash damming in the basins. Other potential drivers of river incision lack a recognized mechanism to cause T1 incision or are not synchronous with T1 incision. Hence, the close temporal correspondence suggests that reduced sediment retention triggered by splash damming led to the observed 1.1 mm·y^{-1} to 23 mm·y^{-1} of bedrock river incision and reduction of the active floodplain to 20% and 53% of its preincision extent on the Middle and West Forks, respectively. The development of such anthropogenic bedrock terraces may be an emerging, globally widespread physiographic signature of the Anthropocene.

Anthropocene | river incision | terrace formation | Pacific Northwest

River systems across North America have been affected by anthropogenic activity. Severe modification of fluvial systems began by at least the late 1600s in the mid-Atlantic and New England regions with mill dams that impounded sediment and caused subsequent incision through alluvial sediments when dams were breached or abandoned (1). Surface erosion, channelization, and abandonment of diversion structures from agriculture and ranching enhanced channel incision and arroyo formation in rivers in the American Midwest and Southwest (2–4), and overgrazing aggravated climatically driven gully incision and erosion in California (5, 6). Construction around urban waterways, followed by continued urbanization, increased peak flows and caused dramatic widening and excavation (7, 8). In the Great Plains, flow regulation at the end of the 19th century narrowed and deepened channels by raising water tables and allowing riparian tree establishment (9).

In contrast, reported evidence for recent, human-induced river incision through bedrock is limited to a few local exposures of strath terraces in the Pacific Northwest (Fig. 1*A*). Saw-cut logs deposited in the alluvium overlying an isolated bedrock (strath) terrace 100 m wide in the West Fork (WF) Satsop River show 1.2 m of bedrock incision post 1940s logging (10). Locally exposed and century-old strath terraces in the Willapa River (11) and WF Teanaway River (12) formed coincident with splash damming, in which cut wood is transported downstream to mills in forceful dam-burst floods. However, these prior observations of bedrock incision are based on local exposures and rely on a few dates to correlate incision with human action.

Here we present evidence of basin-scale incision and strath terrace formation following splash damming, which has removed channel-spanning log jams and limited alluvial cover to channel sides and gravel bars. We hypothesize that splash damming decreased wood loads and associated sediment retention, thereby exposing bedrock to incision and leading to terrace abandonment. We examine, and reject, the alternate hypotheses that terrace formation could have been driven by changes in sediment production associated with the Little Ice Age (LIA) or high-intensity fires that reduced soil strength and infiltration. We find that bedrock incision of up to 2 m began with or slightly after splash damming, implying that the conversion of 20% and 53%, respectively, of the Middle Fork (MF) and WF preincision floodplain to a terrace was driven by human action.

Sediment Retention as a Mechanism of Bedrock River Incision and Terrace Formation

We examine the influence of splash damming on terrace formation through the mechanism of sediment retention, the forced accumulation of channel sediment by relatively immobile channel obstructions such as large wood jams or boulders (12). Existing theory holds that terrace formation, accomplished through channel widening and incision, is controlled by the availability of sediment to cover or abrade bedrock (13, 14). If sediment supply is greater than the transport capacity, an immobile alluvial cover develops and protects the bedrock from erosion, resulting in greater lateral than vertical erosion rates. This lateral planation creates a bedrock strath. The strath is later abandoned when vertical incision rates increase as the transport capacity increases or sediment supply decreases, thinning the alluvial cover and allowing bed load to abrade bedrock. Sediment retention acts to locally increase the sediment cover effect by physically impeding transport and lowering the water surface slope; the presence of retention elements such as

Significance

The degree to which bedrock-floored rivers are shaped by human action is poorly understood in comparison with gravel- and sand-bedded rivers. Yet, bedrock river erosion is thought to set the pace of landscape-scale evolution, and thus any human-induced bedrock erosion has the potential to have a cascading effect and alter both river networks and hillslopes. We show here that artificial dam-burst floods and wood removal in the early 20th century associated with forestry practices caused significant river incision and led to the abandonment of the predisturbance floodplain as a terrace. Although the floods ceased 100 y ago, incision continues in response to decreased wood supply. Short-lived episodes of human action, even in remote mountainous locations, can create long-lasting landscape response.

Author contributions: S.A.S. and D.R.M. designed research; S.A.S., D.R.M., and B.D.C. performed research; S.A.S. analyzed data; and S.A.S., D.R.M., and B.D.C. wrote the paper.

The authors declare no conflict of interest.

This article is a PNAS Direct Submission.

[1]To whom correspondence should be addressed. Email: saschanz@iu.edu.

[2]Present address: Department of Earth and Atmospheric Sciences, Indiana University, Bloomington, IN 47405.

This article contains supporting information online at www.pnas.org/lookup/suppl/doi:10.1073/pnas.1814627116/-/DCSupplemental.

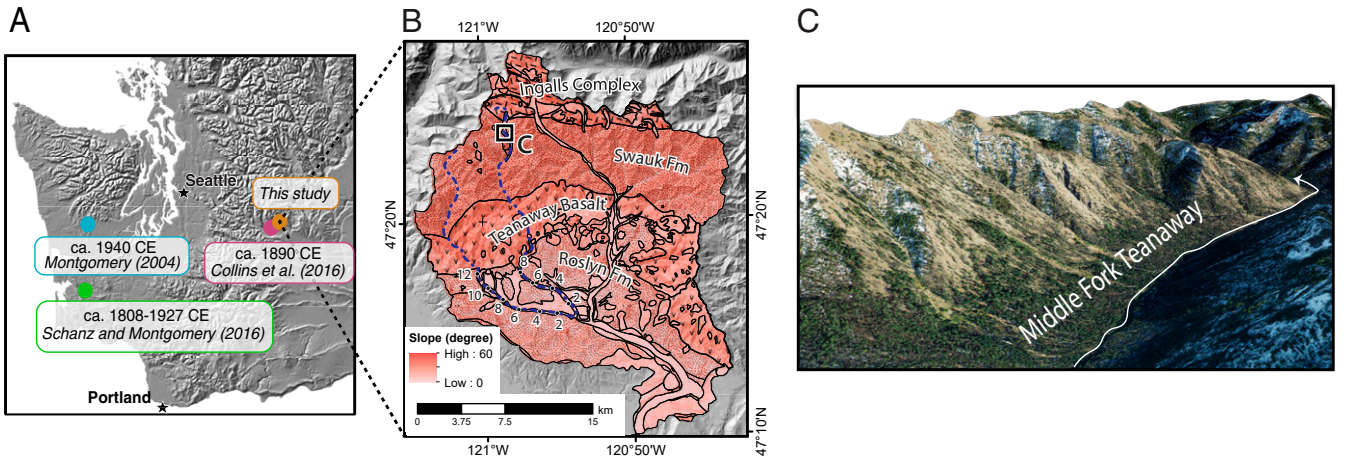

Fig. 1. Study locations. (*A*) Locations of previously studied (refs. 10–12) strath terraces in the Pacific Northwest interpreted to have formed in response to anthropogenic timber harvest and splash damming, including the location of this study. (*B*) The Teanaway River watershed and underlying geologic units. Our study sites are the sections of the MF and WF Teanaway rivers (shown in dashed blue line) that are underlain by the Roslyn Formation between rkm 0 and rkm 8.5 of MF and rkm 0 and rkm 12 of WF. Valley surfaces in the study area are shown in more detail in Fig. 2. Numbers indicate the river kilometer, measured upstream from the MF and WF confluence. (*C*) View downstream of the headwaters of MF, showing typical bare valley walls with debris and avalanche chutes leading to the river. Images courtesy of the U.S. Geological Survey.

log jams can force bedrock channels to become alluvial (15). The loss of log jams and associated decrease in retention has been hypothesized to lead to bedrock incision and terrace formation (12). Our study seeks to provide a regional and well-constrained test on the role of sediment retention in terrace formation, by examining a case where anthropogenic activity decreased retention in the late 19th century.

MF and WF Teanaway Rivers

Our study sites are along the MF and WF Teanaway rivers in the east central Cascade Range of Washington State (Fig. 1*B*). These drainage basins are typically snow-covered during the winter and receive between 980 mm·y^{-1} and 1,230 mm·y^{-1} of precipitation (16). Tectonic activity is low; mapped faults do not offset Quaternary alluvium (17), Holocene denudation in nearby basins is 0.08 mm·y^{-1} (18), and exhumation rates over the last 10^6 to 10^7 y are 0.05 mm·y^{-1} (19). The basin remained deglaciated during the Last Glacial Maximum but, in previous glaciations, was repeatedly overrun by glaciers from the Cle Elum River valley to the west, leaving a 30- to 45-m-high glacial terrace that forms the valley walls and plateaus between the study basins (20) (Fig. 2). Pollen records at Carp Lake in the eastern Cascade Range, a site at a similar elevation (714 m) and 150 km south, suggest the modern *Pinus ponderosa* forest composition was established by 3.9 kya (21).

We focus on the lower portion of the watersheds underlain by the easily eroded and friable sandstones of the Eocene Roslyn Formation (22) from river kilometer (rkm) 0 to rkm 8.5 for the MF and rkm 0 to rkm 12 for the WF (Figs. 1 and 2); the lower 3 km of the WF Teanaway River was previously described in detail (12). Channel bed load in the study site is mostly sourced from the erosion-resistant Teanaway Basalt and sandstone Swauk Formation immediately upstream, as bed load produced by the Roslyn Formation rapidly weathers to sand-size particles (12). Bed load mostly comprises rounded, fluvially transported cobbles, although a debris flow fan contributes bed load locally at rkm 11.8 on the WF. However, tributaries below rkm 11.8 on the WF and rkm 7.7 on the MF drain only Roslyn Formation and do not contribute bed load.

The rivers were splash-dammed from 1892 to 1916 (23, 24). While the number and exact location of splash dams are unknown, 1910 stream gauge reports suggest each fork was dammed at least 13 km upstream of the MF and WF Teanaway rivers' confluence, and newspaper accounts indicate the dams on the MF were above rkm 1.5 (25, 26). Exposed ends of saw-cut logs buried perpendicular to the flow at rkm 6.8 of the MF, similar to the roll dams used to funnel logs downstream of splash dams (27), further suggest that splash dams were located upstream of the study reaches.

Previous work in the Oregon Coast Range and southwest Washington State showed that splash-dam floods simplified channels, removed and redistributed in-channel sediment, and reduced wood loads (27, 28). Although splash damming ceased in the study site in 1916, wood loads remain low; our 2016–2017 surveys identified only 15 jams in the 20-km study reach (<1 jam per km). These jam frequencies are much lower than basin-wide

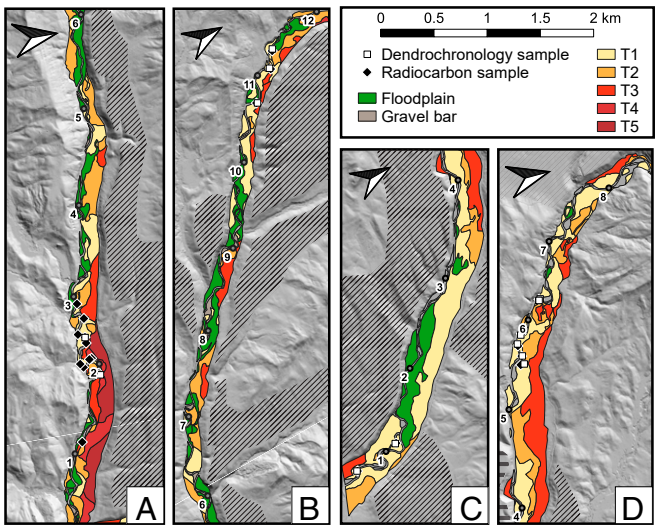

Fig. 2. Terraces in the WF and MF. Geomorphic maps of the (*A* and *B*) WF and (*C* and *D*) MF Teanaway rivers show the extent of terraces and locations of dendrochronology and radiocarbon samples. All panels are at the same scale. Gray circles indicate the river kilometer, measured in upstream distance from the confluence of the MF and WF Teanaway rivers. Hatched regions mark the extent of the 30- to 45-m-high valley-bounding glacial terrace formed in the penultimate glaciation. Arrows point north.

averages in the Yakima, Wenatchee, and Methow rivers, all located in the east-central Washington Cascade Range, of 3.5 jams per km to 12.3 jams per km in watersheds managed by the US Forest Service and 8.1 jams per km to 13.8 jams per km in unmanaged watersheds (29). While we do not know the jam frequency of the MF and WF Teanaway rivers before splash damming, a late 19th century report shows at least one large jam complex 6 m deep by 275 m long (30). That wood loads remain much lower than in nearby streams is consistent with the hypothesis that sediment retention has decreased and remained low since splash damming commenced in 1892.

Extent and Timing of River Incision

To examine when river incision began, we mapped and dated the lowest river terrace, termed T1, which was previously studied from rkm 0 to rkm 3 in the WF (12); we expanded this mapping throughout our study area to test the regional extent of T1. T1 occupies 44% of the mapped MF valley bottom and 21% of the WF valley bottom (Fig. 2) and is present as both a bedrock strath and alluvial terrace. In places, the strath dips below or at the channel bed elevation, transitioning T1 from a strath to an alluvial terrace while keeping a flat terrace tread (Fig. 3). The similarity in average height—measured from the average channel bed—between the incisional T1 strath terraces (2.2 ± 0.7 m for MF and 1.9 ± 0.6 m for WF, given as mean ± SD) and the alluvial terraces (1.9 ± 0.7 m for MF and 1.9 ± 0.6 m for WF, given as mean ± SD) suggests the T1 alluvial terrace segments, which likely are underlain by a strath at the current channel bed elevation, record incision rather than floodplain height variability. Additionally, T1 is distinctly higher than both the active floodplains (0.8 ± 0.6 for MF and 1.2 ± 0.6 for WF) and gravel bar tops (0.8 ± 0.7 for MF and 0.9 ± 0.5 for WF). T1 is continuous through the study reach (Fig. 2 and *SI Appendix*, Fig. S1) and notably extends through knickzones in the lower 1 km of the MF and lower 3 km of the WF. That the knickzones do not affect T1 incision shows that the driver of incision is basin-scale. Moreover, the presence of T1 on both the inside and outside banks of meanders indicates T1 did not form primarily by meander cutoff (31) or migration (32, 33).

River incision abandoned T1 from an active fluvial surface to a stable surface. To constrain when incision occurred, we used radiocarbon from charcoal and plant fragments found within the alluvium above the T1 strath to determine when T1 was an active surface. We paired this with dendrochronology of the oldest tree on each surface to estimate when river incision had progressed such that T1 was a stable site for tree seedlings. Radiocarbon dates from alluvium associated with the T1 strath in both rivers range up to 1450 CE but cluster between 1650 CE and 1900 CE (Fig. 4 and *SI Appendix*, Table S1). Charcoal and wood fragments potentially represent recycled detritus or old trees, so the true depositional age could be younger than the carbon age. However, the oldest estimate of T1 occupation age at 1650 CE is constrained by a radiocarbon date from a buried leaf in a flood layer that is unlikely to be recycled detritus or be affected by tree carbon stock. Thus, radiocarbon ages indicate the strath remained an active fluvial surface from at least 1650 CE until *ca*. 1900 CE, giving a minimum strath planation length of ~250 y. Tree cores indicate T1 had been abandoned by at least 1970–1991 CE for the WF and 1893–1937 CE for the MF Teanaway River. Overall, the age constraints are similar for the MF and WF and consistent with roughly synchronous T1 incision between the two valleys.

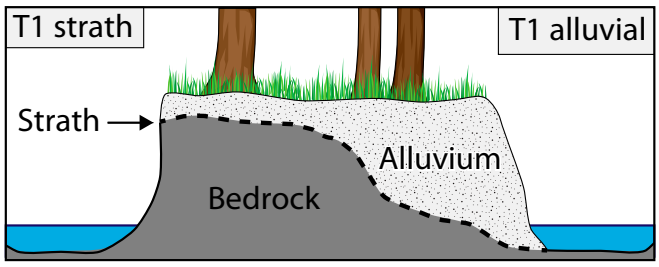

Fig. 3. Schematic representation of terrace relationships. T1 can often be traced continuously as both a strath and an alluvial terrace due to meter-scale fluctuations in the strath bedrock surface.

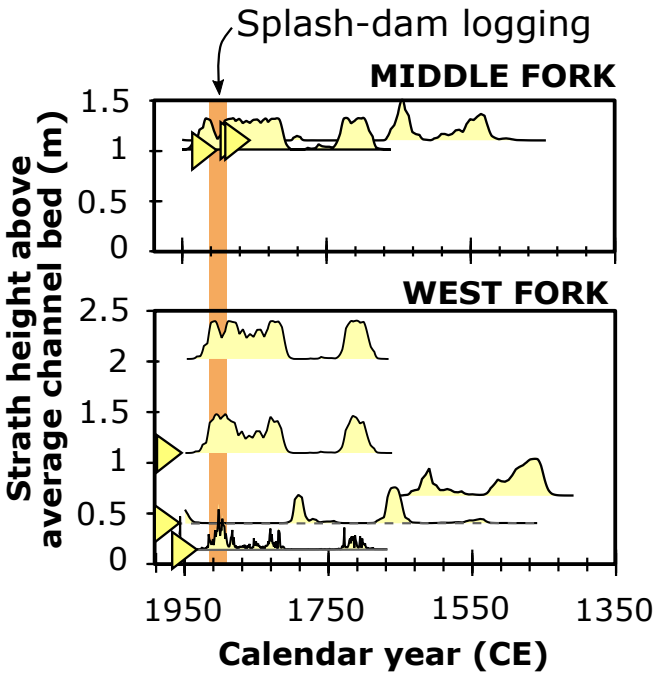

Fig. 4. Timing of T1 incision. The timing of T1 incision along the MF and WF Teanaway rivers is constrained by radiocarbon dates, presented as distribution functions of the calibrated age before present, and dendrochronology, given as arrows wherein the left edge is aligned with tree age. The height of the bedrock strath is above the average channel bed, derived from field surveys, and is aligned to the bottom edge of each radiocarbon age and the midpoint of the tree age. Each age distribution shows a single sample, and variance in the sample height reflects different cumulative incision.

Possible Drivers of River Incision

Our age constraints place T1 incision at ~1900 CE for the MF and 1900–1970 CE for the WF. Conservative estimates of bed load transport rates suggest that a 1-m-thick alluvial cover, an upper bound of the preincision channel bed load depth estimated from T1 deposits, would be evacuated from the channel within 5 y to 10 y under the current discharge, slope, and sediment supply regime (Fig. 5). This suggests the exposure of channel bedrock and onset of incision was likely very rapid after the initial system perturbation. The rapid response aligns with our hypothesis that splash-dam flooding from 1892 to 1916 decreased sediment retention and exposed bedrock to erosion, because the timing of splash-dam flooding is coincident with terrace abandonment. Additionally, our numerical modeling showed that the channel slope is too steep to accumulate bed load (Fig. 5), and, in the absence of a change in discharge or sediment supply, bed load cannot accumulate unless slope is lowered, either by erosion or by addition of log jams. Buried jams on the T1 strath are evidence that jams were present during T1 planation, and the scarcity of current jams attests to a decrease in sediment retention.

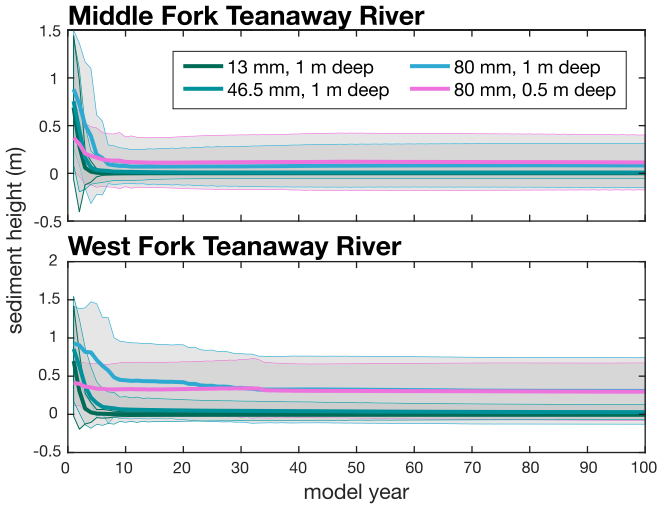

Fig. 5. Numerical model simulating loss of sediment cover. Average channel sediment height through time following splash damming is shown for several model scenarios in which average grain size is varied from 13, 46.5, and 80 mm based on different prior estimates, and the initial sediment depth at the start of the simulation is varied from 0.5 m to 1 m, based on field observations of sediment thickness on T1. Sediment height is shown averaged over each study region, with 1 SD shown by the shaded region. Model year 0 corresponds to ∼1892 CE, when splash damming began.

Alternatively, the incision of T1 could have been caused by an increase in discharge or decrease in sediment supply at ∼1900 CE that would lead to channel bed exposure. River incision from fluctuations in sediment supply and transport is often associated with climatic changes (34); in our study site, the onset of T1 incision aligns with the end of the LIA at *ca*. 1890–1900 CE. The Washington Cascade Range, in which the Teanaway basin is located, was ∼1 °C cooler from *ca*. 1690 CE to 1900 CE (35) and had greater snowpack from *ca*. 1650 CE to 1890 CE (36). Erosion rates and sediment production could have been amplified by increased frost cracking during the LIA. However, the change in mean annual temperature (MAT) associated with the LIA of 1 °C and the amplitude of seasonal temperature variation of 10 °C would not increase the frost-cracking intensity (37). Thus, we do not expect erosion rates and bed load would have increased during the LIA from enhanced frost cracking.

Could the rate of sediment delivery from hillslopes to channels have been altered by greater snowpack during the LIA? Visual evidence in the upper MF and WF Teanaway valleys suggests hillslope sediment is transported to the channel by debris flows and snow avalanches (Fig. 1*C*). However, debris flow frequency has been found to decline during the LIA in the Swiss Alps; with a thicker and longer-lasting snowpack, precipitation events interact less frequently with the regolith to create debris flows (38). In contrast, such conditions led to more frequent avalanches during the LIA but at a shallower failure plane (39, 40). Shallow avalanches are less likely to entrain ground material, so sediment supply to the MF and WF Teanaway rivers likely declined during the LIA. Thus, the end of the LIA would have been associated with a relative increase in sediment delivery and increased potential for bedrock cover, which is counter to the observation of increased bedrock exposure and incision *ca*. 1900 CE.

The dominant internal natural disturbance in the Teanaway basin is forest fire (41), and a basin-wide fire could drive an increase in discharge through decreased evapotranspiration and enhanced runoff over hydrophobic soils (42), basin-scale changes in sediment supply from fire-enhanced erosion (43, 44), or increased sediment mobility through a reduction in wood supply and sediment retention. Studies in neighboring watersheds in the eastern Cascade Range have shown that, while postfire runoff increases ∼50%, hillslope erosion and sediment production rates increase to 8 to 10 times prefire values and thus dominate the postfire geomorphic response (42). High-intensity burned areas, in which trees are consumed, are typically 0.1 km^2 to 1.0 km^2 in the lower Teanaway basin (41), so a significant basin-wide reduction in channel wood loads and associated sediment retention is not expected. Hence, an increase in sediment production is a more likely effect of forest fires in our study site; however, large fires occur every 300 y to 350 y in the bed load-producing upper Teanaway basin (45, 46) which implies ∼300 y to 350 y of relatively low sediment supply punctuated by periods of relatively high sediment supply and terrace planation. Our radiocarbon dates for T1 planation range ∼250 y (Fig. 4), which is not consistent with a rapid and short sediment response to fires.

Thus, the timing of T1 incision is not readily explained either by changes in sediment supply associated with fires, the major disturbance in the Teanaway basin (41), or by the climatic forcing most often associated with terrace formation (34). In contrast, the hypothesis that decreased sediment retention caused T1 incision due to the removal of in-stream wood during splash damming offers a viable mechanism for bedrock incision at *ca*. 1900 CE. Moreover, recent strath terraces formed on rivers elsewhere in the region cannot be explained by sediment supply changes associated with the LIA, but are coincident with splash damming; anthropogenic terraces in the WF Satsop River formed 50 y after the LIA, *ca*. 1940 CE (10), and terraces in the Willapa River basin that formed coincident with splash damming (11) are sourced from low-elevation hills unlikely to have been significantly affected by LIA-associated changes to sediment production.

Anthropogenic Effects on the Teanaway Landscape

Based on the regional evidence linking bedrock river incision to splash damming and the lack of a clear mechanism for an LIA or fire driver of T1 incision, we conclude that T1 incised as a result of splash damming and reduced sediment retention. Anthropogenic bedrock river incision rates of 1.1 $mm{\cdot}y^{-1}$ to 23 $mm{\cdot}y^{-1}$ on the MF and WF Teanaway rivers are calculated using the lowest and highest T1 strath heights and the onset and end of splash damming. The range of incision rates reflects different total incision amounts, as seen by the range of strath heights in Fig. 4. Variable strath heights may reflect differences in the bedrock strength—the sandstone of the Roslyn Formation is interbedded with siltstone, coal, and conglomerate layers—or be caused by variation in the original height of the bedrock strath, reflective of paleo channels and bedrock knobs. While these rates of incision are quite rapid, they agree with direct measurements of bedrock erosion taken in the lower 3 km of the WF from 1999 CE to 2003 CE of 10.9 $mm{\cdot}y^{-1}$ on average (12). Late Holocene average bedrock incision rates measured from older WF Teanaway terraces are lower, at 1.3 ± 0.3 $mm{\cdot}y^{-1}$ and 1.4 ± 0.5 $mm{\cdot}y^{-1}$ (12), incorporating periods of both planation and incision.

Incision of T1 has lasted comparatively longer than that of older WF Teanaway terraces T3 and T2. Incision of T3 occurred over a short period indistinguishable in radiocarbon ages, with a longer planation length of ∼460 y (12). T2 was planed for 12 times as long as it was incised (12). In contrast, our ages for T1 suggest the terrace was planed for only twice as long as it was incised, with incision continuing to the present day. The present scarcity of wood jams suggests sediment retention will remain low. Although the banks are forested, recruitment of riparian trees as channel wood requires lateral erosion through entrenched bedrock banks, which is likely to slow the rate of wood recruitment and jam development in comparison with preincision conditions. This implies incision will continue until a decreased slope due to channel entrenchment or an increase to sediment supply (or to the

retention of sediment) causes in-channel sediment deposition and the reestablishment of an alluvial cover.

The formation of T1 in the MF and WF Teanaway rivers in response to human action, combined with the evidence of terrace formation in the WF Satsop and Willapa rivers, shows a regional human impact on bedrock river incision. River incision into alluvium in response to human action has been well documented (9), but that bedrock river incision can result from human action at timescales under a century introduces new issues to consider in human-altered landscapes. For example, groundwater response to alluvial river incision has been documented elsewhere to be significant at 1-m or greater incision (47), but, to our knowledge, the impact of bedrock incision on groundwater drawdown has yet to be quantified. Within the MF and WF Teanaway valleys, this most recent cycle of incision respectively decreased the rivers' floodplain areas to 20% and 53% of their preincision areas and resulted in a loss of floodplain habitat and floodplain–channel connectivity.

The morphologic changes in the Teanaway valleys demonstrate the importance of anthropogenically induced changes in sediment retention. Wood clearing and harvesting were ubiquitous in forested regions worldwide starting as early as 7 kya in some regions (48), and a broad global correspondence between late Holocene strath terrace formation and regional deforestation (34) suggests floodplain abandonment from sediment retention loss may have been more pervasive than previously recognized in deforested watersheds around the world. As such, the topographic response to reduced sediment retention may be creating a global physiographic signature of the Anthropocene in the form of bedrock strath terraces and the transformation of floodplain landforms.

Methods

Geomorphic Mapping. Bedrock strath terraces were mapped in field campaigns from 2015 to 2017, and floodplain surfaces were identified in the field based on the presence of flood debris, tree size, and forest seral stage. The lowest (T1) terrace was identified by the mixed coniferous and deciduous tree cover and greater presence of overbank channels compared with higher terraces, and a lack of flood debris compared with floodplain surfaces. We verified that mapped T1 surfaces were above the active channel by estimating bankfull stage using the height of gravel bars having 1- to 2-y-old vegetation and thus assumed to be active during bankfull flows. We also compared T1 surface height with the height of the bedrock trimline formed on bedrock valley walls when the high-flow channel erodes weathered bedrock. We used radiocarbon dates from T1 surfaces to correlate our T1 mapping within and between the MF and WF Teanaway valleys (*SI Appendix*, Table S1). Higher terraces were identified based on the height and continuation of surfaces. Terrace height in the field was estimated using hand levels and a reference topographic map derived from light detection and ranging (LiDAR). Soil development on the terraces is weak, and overbank sedimentation rates are low, so soil development and thickness could not be used to correlate terrace sequences.

The field map of terraces produced from the above methods was expanded to cover the entire study site using LiDAR flown in April to May 2015 (49). The LiDAR dataset is topobathymetric and thus accurately captures the channel bed surface with 0.006-m vertical accuracy in submerged and nearshore areas and 0.082-m average vertical accuracy overall. In comparison, surveyed heights of terraces relative to the bed are 1.0 m or greater, indicating the LiDAR dataset can accurately delineate terraces from the channel bed. We constructed height above water surface (HAWS) maps from the LiDAR bare-earth elevation model using the Triangular Irregular Network interpolation methodology (50). We used the average channel elevation rather than average water surface as the base level, because we were interested in channel incision. The HAWS maps were used to extrapolate field mapping to the entire study site (Fig. 1). To verify the accuracy of our remote mapping, we compared the height of strath terraces mapped in the field with terraces mapped from the HAWS map. In each case, terrace height was generated from the LiDAR data and is relative to the average channel bed elevation.

Dating Terrace Incision. We used paired dendrochronology and radiocarbon samples to constrain the timing of terrace incision. The charcoal and plant matter sampled for radiocarbon dating was deposited in the basal alluvium overlying the strath when the strath was an active fluvial surface, and thus predates incision. Tree cores were preferentially taken from *Pseudotsuga menziesii* and *P. ponderosa*, which are documented to grow on inactive floodplains and terraces in forests in the eastern Cascade Range (51); where possible, we avoided early seral-stage trees such as *Alnus rubra* or *Populus trichocarpa*. In total, we collected 14 cores: nine of *P. menziesii*, three of *P. ponderosa*, one of *Abies procera*, and one of *A. rubra*. Tree cores were taken from the largest-diameter trees on each surface to estimate the earliest time when the surface stabilized. This ensured that our tree ring ages represented inactive surfaces and constrained a postincision age. Ages and locations are reported in *SI Appendix*, Table S1 (radiocarbon) and *SI Appendix*, Table S2 (dendrochronology). Tree cores were photographed, the rings were counted, and a subset of cores with indistinct rings were mounted and sanded with coarse and fine sandpaper before being photographed. Adjacent to the cored tree, charcoal and plant matter were collected in the basal alluvium overlying the strath and dated using accelerator mass spectrometry. Radiocarbon ages were calibrated using the Calib 7.0.2 (52) calibration curves (53, 54). We also included four prior radiocarbon ages from T1 terraces on the lower 3 km of the WF Teanaway River (12).

Late Holocene incision rates are calculated using the average incision rate, minimum estimate of terrace planation, and estimate of terrace incision length. The oldest dated terrace on the WF, T3, was planed for at least 460 y and incised for ∼112 y, based on radiocarbon dates in ref. 12. The middle terrace set on the WF, T2, is similarly constrained by radiocarbon dates to have been planed for 840 y, with an unknown length of incision. Our dates suggest the final and youngest terrace, T1, was planed for 350 y and incised for at least 128 y (1890 CE to present). Average incision rates of T3 and T2 are 1.3 ± 0.3 and 1.4 ± 0.5 mm·y^{-1} and T1 incision rates range from 1.1 mm·y^{-1} to 23 mm·y^{-1}. We then solved for T3 and T2 incision rates by calculating the average incision rate as the average of the planation time and incision rate (the latter assumed to be 0 mm·y^{-1}) and the incision time and rate.

Midvalley Profile. The active channel and terrace treads were mapped onto a valley longitudinal profile using ArcGIS and the LiDAR dataset. We constructed a midvalley line in the mainstem, WF, and MF Teanaway rivers and drew a perpendicular cross-valley line every 100 m. The cross-valley line was populated with elevation values from the LiDAR dataset using the Extract Surface Information tool in ArcGIS and then intersected with mapped polygons representing the terraces, floodplain, and active channel. From this intersection, the average value of each terrace, the floodplain, and the channel at each cross-valley line was calculated. The average values at each cross-valley line were exported from ArcGIS and plotted against midvalley distance, using Matlab.

Estimate of Frost Cracking. The potential for an increase in frost-cracking and erosion rates during the LIA was assessed using the annual temperature amplitude (one-half the range in mean monthly temperature) and MAT, following the methods in ref. 37. Mean monthly temperatures for 1895 to present were found using parameter-elevation regressions on independent slopes model (PRISM) data at Westmap (https://cefa.dri.edu/Westmap), and MAT was found from https://www.usclimatedata.com/ for the nearest city of Cle Elum, WA, for 1981–2010. LIA temperature and precipitation are estimated from tree ring growth records in a Washington Cascade Range basin, and show a 1 °C cooler MAT during the LIA (35). Using figure 4 of ref. 37, we plotted amplitude and MAT to determine the frost-cracking intensity in degree days. Values of amplitude and MAT of (10, 8) for the present day and (10, 7) for LIA fall in the zone of 0 °C day, indicating no change in frost-cracking potential between the LIA and the present day.

Sediment Transport Time. We estimated the timing of bed load sediment loss in the MF and WF Teanaway rivers with a 1D finite difference model. The channel profile was set using the current longitudinal profile; comparison of T1 tread and current channel slopes indicated they are not significantly different under a two-tailed *t* test (*P* value of 0.66 for MF and 0.66 for WF). The 1D channel topography was extracted from LiDAR between rkm 0 and rkm 8.5 (MF) and rkm 0 and rkm 12 (WF) at 100-m intervals. At the top of the profile, representing the transition from the bed load-producing upper basin to the study site, we estimated annual sediment contribution based on total contributing area and measured denudation rates of 0.08 mm·y^{-1} (18). No bed load was supplied within the study reach, because bedrock in the study site rapidly weathers to sand-size particles or smaller (12). Bankfull discharge, height, and width were estimated using the scaling parameters of ref. 55 for Western Cordillera streams, which gave similar values to those reported in ref. 12. Sediment transport capacity was calculated using a modified Meyer–Peter Mueller equation (56, 57), with a critical shear stress

of 0.0495 (57). Model runs started with 1892 CE initial conditions and ran for 100 y. Initial sediment thickness in 1892 CE is unknown, although sediment thickness on T1 terraces can range from 0.5 m to 1 m. Current bed load size ranges from a median of 61.5 mm to 80 mm on gravel bars (12) and 13.1 mm to 18.6 mm in the subsurface (58). Gage records from 1909 to 1913 at US Geological Survey gauge 12480500 indicate 2 $d{\cdot}y^{-1}$ to 21 $d{\cdot}y^{-1}$ were above bankfull flow. We ran a conservative model in which initial sediment depth was 1 m at all nodes, bankfull flow was 2 $d{\cdot}y^{-1}$, and bed load median size was 80 mm and 13.1 mm, representing the maximum and minimum estimates. A third scenario with bed load size of 46.5 mm was also run, as well as an initial sediment depth of 0.5 m and 80 mm bed load. From each model scenario, we extracted the volume of sediment in the study reach during each time step, as well as the sediment depth at each node.

ACKNOWLEDGMENTS. Discussions with J. O'Connor and A. Duvall helped shape this paper. We thank T. Hillebrand, A. Pacubas, R. Pflager, A. Rusman, and L. Thompson for their field assistance. Insightful comments from two anonymous reviewers helped improve this paper. Material analysis and field support was provided to S.A.S. and D.R.M. from National Science Foundation Grant BCS-1632977 and research funds from the Quaternary Research Center and the Department of Earth and Space Sciences at the University of Washington.

1. Walter RC, Merritts DJ (2008) Natural streams and the legacy of water-powered mills. *Science* 319:299–304.
2. Knox JC (2006) Floodplain sedimentation in the Upper Mississippi Valley: Natural versus human accelerated. *Geomorphology* 79:286–310.
3. Nichols MH, Magirl C, Sayre NF, Shaw JR (2018) The geomorphic legacy of water and erosion control structures in a semiarid rangeland watershed. *Earth Surf Process Landf* 43:909–918.
4. Waters MR, Haynes CV (2001) Late Quaternary arroyo formation and climate change in the American Southwest. *Geology* 29:399–402.
5. Montgomery DR (1999) Erosional processes at an abrupt channel head: Implications for channel entrenchment and discontinuous gully formation. *Incised River Channels*, eds Darby S, Simon A (John Wiley, New York), pp 247–276.
6. Perroy RL, Bookhagen B, Chadwick OA, Howarth JT (2012) Holocene and Anthropocene landscape change: Arroyo formation on Santa Cruz Island, California. *Ann Assoc Am Geogr* 102:1229–1250.
7. Trimble SW (1997) Contribution of stream channel erosion to sediment yield from an urbanizing watershed. *Science* 278:1442–1444.
8. Wolman MG (1967) A cycle of sedimentation and erosion in urban river channels. *Geogr Ann Ser A* 49:385–395.
9. Montgomery DR, Wohl EE (2003) Rivers and riverine landscapes. *The Quaternary Period in the United States*, Developments in Quaternary Sciences, eds Gillespie AR, Porter SC, Atwater BF (Elsevier, New York), pp 221–246.
10. Montgomery DR (2004) Observations on the role of lithology in strath terrace formation and bedrock channel width. *Am J Sci* 304:454–476.
11. Schanz SA, Montgomery DR (2016) Lithologic controls on valley width and strath terrace formation. *Geomorphology* 258:58–68.
12. Collins BD, Montgomery DR, Schanz SA, Larsen IJ (2016) Rates and mechanisms of bedrock incision and strath terrace formation in a forested catchment, Cascade Range, Washington. *Geol Soc Am Bull*, 128: pp 926–943.
13. Sklar LS, Dietrich WE (2001) Sediment and rock strength controls on river incision into bedrock. *Geology* 29:1087–1090.
14. Hancock GS, Anderson RS (2002) Numerical modeling of fluvial strath-terrace formation in response to oscillating climate. *Geol Soc Am Bull* 114:1131–1142.
15. Montgomery DR, et al. (1996) Distribution of bedrock and alluvial channels in forested mountain drainage basins. *Nature* 381:587–589.
16. U.S. Geological Survey (2012) The StreamStats program for Washington. Available at https://water.usgs.gov/osw/streamstats/Washington.html. Accessed January 5, 2018.
17. Washington Division of Geology and Earth Resources (2014) Surface geology, 1:24,000–GIS data, June 2014. Available at www.dnr.wa.gov/publications/ger_portal_surface_geology_24k.zip. Accessed June 20, 2014.
18. Moon S, et al. (2011) Climatic control of denudation in the deglaciated landscape of the Washington Cascades. *Nat Geosci* 4:469–473.
19. Reiners PW, Ehlers TA, Mitchell SG, Montgomery DR (2003) Coupled spatial variations in precipitation and long-term erosion rates across the Washington Cascades. *Nature* 426:645–647.
20. Porter SC (1976) Pleistocene glaciation in the southern part of the North Cascade Range, Washington. *Geol Soc Am Bull* 87:61–75.
21. Whitlock C, Bartlein PJ (1997) Vegetation and climate change in northwest America during the past 125 kyr. *Nature* 388:57–61.
22. Tabor RW, et al. (1982) Geologic map of the Wenatchee 1:100,000 quadrangle, central Washington (US Geol Survey, Reston, VA).
23. Kittitas County Centennial Committee (1989) *A History of Kittitas County, Washington* (Taylor, Dallas).
24. Cle Elum Tribune (March 20, 1891) General happenings. *Cle Elum Tribune*, p 4.
25. Henshaw FF, La Rue EC, Stevens GC (1913) *Surface Water Supply of the United States, 1910: Part 12. North Pacific Coast* (U.S. Gov Printing Office, Washington, DC).
26. McGiffin J (1980) *Hometown Heritage: A Remembered History of 1910 in Kittitas County, Washington* (Daily Record, Ellensburg, WA).
27. Wendler HO, Deschamps G (1955) Logging dams on coastal Washington streams. *Fisheries Res Pap* 1:27–38.
28. Sedell JR, Luchessa KJ (1982) Using the historical record as an aid to salmonid habitat enhancement. *Symposium on Acquisition and Utilization of Aquatic Habitat Information*, ed Armantrout NB (Amer Fisheries Soc, Bethesda).
29. McIntosh BA, et al. (1994) Management history of eastside ecosystems: Changes in fish habitat over 50 years, 1935–1992 (US Dep Agric, Portland, OR), General Technical Report PNW-GTR-321.
30. Russell IC (1898) *Rivers of North America* (G. P. Putnam's Sons, New York).
31. Finnegan NJ, Dietrich WE (2011) Episodic bedrock strath terrace formation due to meander migration and cutoff. *Geology* 39:143–146.
32. Limaye ABS, Lamb MP (2016) Numerical model predictions of autogenic fluvial terraces and comparison to climate change expectations. *J Geophys Res Earth Surf* 121: 512–544.
33. Merritts DJ, Vincent KR, Wohl EE (1994) Long river profiles, tectonism, and eustasy: A guide to interpreting fluvial terraces. *J Geophys Res Solid Earth* 99:14031–14050.
34. Schanz SA, Montgomery DR, Collins BD, Duvall AR (2018) Multiple paths to straths: A review and reassessment of terrace genesis. *Geomorphology* 312:12–23.
35. Graumlich LJ, Brubaker LB (1986) Reconstruction of annual temperature (1590–1979) for Longmire, Washington, derived from tree rings. *Quat Res* 25:223–234.
36. Pederson GT, et al. (2011) The unusual nature of recent snowpack declines in the North American Cordillera. *Science* 333:332–335.
37. Marshall JA, et al. (2015) Frost for the trees: Did climate increase erosion in unglaciated landscapes during the late Pleistocene? *Sci Adv* 1:e1500715.
38. Stoffel M, Beniston M (2006) On the incidence of debris flows from the early Little Ice Age to a future greenhouse climate: A case study from the Swiss Alps. *Geophys Res Lett* 33:L1640.
39. Naisbitt A, Forster R, Birkeland KW, Harrison WL (2008) Avalanche frequency and magnitude: Using power-law exponents to investigate snow avalanche size proportions through time and space. *Proceedings of the International Snow Science Workshop*. (Montana State Univ Library, Bozeman), Abstract P8119.
40. Jomelli V, Pech P (2004) Effects of the Little Ice Age on avalanche boulder tongues in the French Alps (Massif des Ecrins). *Earth Surf Process Landf* 29:553–564.
41. Wright CS, Agee JK (2004) Fire and vegetation history in the eastern Cascade Mountains, Washington. *Ecol Appl* 14:443–459.
42. Helvey JD (1980) Effects of a north central Washington wildfire on runoff and sediment production. *J Am Water Resour Assoc* 16:627–634.
43. Benda L, Miller D, Bigelow P, Andras K (2003) Effects of post-wildfire erosion on channel environments, Boise River, Idaho. *For Ecol Manage* 178:105–119.
44. Pierce JL, Meyer GA, Rittenour T (2011) The relation of Holocene fluvial terraces to changes in climate and sediment supply, South Fork Payette River, Idaho. *Quat Sci Rev* 30:628–645.
45. Agee JK (1996) *Fire Ecology of Pacific Northwest Forests* (Island Press, Washington, DC).
46. Agee JK (1994) *Fire and Weather Disturbances in Terrestrial Ecosystems of the Eastern Cascades* (US Dep Agric, Portland, OR).
47. Bravard J-P, et al. (1997) River incision in south-east France: Morphological phenomena and ecological effects. *Regul Rivers Res Manage* 13:75–90.
48. Cremaschi M, Nicosia C (2012) Sub-boreal aggradation along the Apennine margin of the Central Po Plain: Geomorphological and geoarchaeological aspects. *Géomorphol Relief Processus Environnement* 18:155–174.
49. Quantum Spatial (2015) Teanaway streams topobathymetric LiDAR. Available at pugetsoundlidar.ess.washington.edu/lidardata/metadata/pslc2015/teanaway/teanaway_2015_be.html. Accessed May 16, 2018.
50. Olson P (2012) *Quality Assurance Project Plan for: Channel Migration Assessments of Puget Sound SMA Streams* (Washington Dep Ecology, Olympia).
51. Kovalchik BL, Region USFSPN (1987) *Riparian Zone Associations: Deschutes, Ochoco, Fremont, and Winema National Forests* (US Dep Agric, Portland, OR).
52. Stuiver M, Reimer PJ (1993) Extended 14C data base and revised CALIB 3.014 C age calibration program. *Radiocarbon* 35:215–230.
53. Reimer PJ, et al. (2013) IntCal13 and Marine13 radiocarbon age calibration curves 0–50,000 years cal BP. *Radiocarbon* 55:1869–1887.
54. Stuiver M, et al. (1998) INTCAL98 radiocarbon age calibration, 24,000–0 cal BP. *Radiocarbon* 40:1041–1083.
55. Castro JM, Jackson PL (2001) Bankfull discharge recurrence intervals and regional hydraulic geometry relationships: Patterns in the Pacific Northwest, USA. *J Am Water Resour Assoc* 37:1249–1262.
56. Meyer-Peter E, Müller R (1948) Formulas for bed-load transport. Available at https://repository.tudelft.nl/islandora/object/uuid:4fda9b61-be28-4703-ab06-43cdc2a21bd7?collection=research. Accessed November 12, 2018.
57. Wong M, Parker G (2006) Reanalysis and correction of bed-load relation of Meyer-Peter and Müller using their own database. *J Hydraul Eng* 132:1159–1168.
58. Watson G (1991) *Analysis of Fine Sediment and Dissolved Oxygen in Spawning Gravels of the Upper Yakima River Basin* (Dep Fisheries, Olympia, WA).